Available online at www.sciencedirect.com
ScienceDirect
Nuclear Instruments and Methods in Physics Research B 266 (2008) 335–346
NIM B Beam Interactions with Materials & Atoms
www.elsevier.com/locate/nimb

Pulsed source of ultra low energy positive muons for near-surface μSR studies

Pavel Bakule [a,*], Yasuyuki Matsuda [a], Yasuhiro Miyake [b], Kanetada Nagamine [b,1], Masahiko Iwasaki [a], Yutaka Ikedo [b,2], Koichiro Shimomura [b], Patrick Strasser [b], Shunshuke Makimura [b]

[a] *Advanced Meson Science Laboratory, RIKEN Nishina Center, RIKEN, Wako, Saitama 351-0198, Japan*
[b] *Muon Science Laboratory, Institute of Materials Structure Science, High Energy Accelerator Research Organization, Tsukuba, Ibaraki 305-0801, Japan*

Received 5 July 2007; received in revised form 8 October 2007
Available online 21 November 2007

Abstract

We have produced a pulsed beam of low energy (ultra slow) polarized positive muons (LE-μ^+) and performed several demonstration muon spin rotation/relaxation (μSR) experiments at ISIS RIKEN-RAL muon facility in UK. The energy of the muons implanted into a sample is tuneable between 0.1 keV and 18 keV. This allows us to use muons as local magnetic microprobes on a nanometre scale. The control over the implantation depth is from several nanometres to hundreds of nanometres depending on the sample density and muon energy. The LE-μ^+ are produced by two-photon resonant laser ionization of thermal muonium atoms. Currently ~15 LE-μ^+/s with 50% spin polarization are transported to the μSR sample position, where they are focused to a small spot with a diameter of only 4 mm. The overall LE-μ^+ generation efficiency of 3×10^{-5} is comparable to that obtained when moderating the muon beam to epithermal energies in simple van der Waals bound solids. In contrast to other methods of LE-μ^+ generation, the implantation of the muons into the sample can be externally triggered with the duration of the LE-μ^+ pulse being only 7.5 ns. This allows us to measure spin rotation frequencies of up to 40 MHz.
© 2007 Elsevier B.V. All rights reserved.

PACS: 76.75.+i; 07.77.Ka; 36.10.Dr; 32.80.Rm; 41.75.–i; 42.65.Ky

Keywords: Low energy muons; Ultra slow muons; Muon spin rotation; Muonium generation; Muonium ionization; Vacuum-ultraviolet laser; Lyman-α; Thin film

1. Introduction

Spin polarized LE-μ^+ are an important tool in condensed matter research for studying implantation-depth-dependent properties of thin samples, nanomaterials, multilayered thin films, or superconductors. The implantation depth can be easily controlled on a scale ranging from several nanometres to hundreds of nanometres by re-accelerating LE-μ^+ from eV energies to tens of keV in an electrostatic field. Using the technique of μSR (muon spin rotation and relaxation) [1,2] the beam of LE-μ^+ with well-defined initial spin polarization can be used as a depth sensitive microscopic magnetic probe to measure local magnetic fields or spin fluctuations. Alternatively, in samples where it can bind to an electron to form muonium (Mu), the muonium can act as a light hydrogen-like probe that can be studied with the μSR technique.

* Corresponding author. Tel.: +44 1235445256; fax: +44 1235446881.
E-mail address: p.bakule@rl.ac.uk (P. Bakule).
[1] Present address: (1) Atomic Physics Laboratory, RIKEN, Wako, Saitama 351-0198, Japan. (2) Physics Department, University of California Riverside, Riverside, CA 92521, USA.
[2] Present address: Toyota Central R&D Labs. Inc., 41-1 Yokomichi, Nagakute, Aichi 480-1192, Japan.

0168-583X/$ - see front matter © 2007 Elsevier B.V. All rights reserved.
doi:10.1016/j.nimb.2007.11.009

Over the past 10 years there has been a significant effort to develop an efficient method of LE-μ^+ generation from the surface muon beams with kinetic energies around 4 MeV available at various muon facilities [3–7].

A successful technique for generation of LE-μ^+ has been developed using a continuous muon source at the Paul Scherrer Institute (PSI) in Switzerland. This method, generating LE-μ^+ with epithermal energies down to 15 eV without any loss of spin polarization, is based on the moderation of surface muons in wide band gap insulators. Particularly suitable as moderators are van der Waals bound solids, such as solid argon, neon or nitrogen. Most reliable and efficient so far has been moderation in a thin solid nitrogen layer grown on a microstructured silver substrate with large surface area. With such a target, the efficiency of converting incident muons to LE-μ^+ and transporting them to the sample is as high as 3×10^{-5} [8].

We have been developing an alternative technique at the RIKEN-RAL muon facility [9] located at the Rutherford Appleton Laboratory (UK) using a pulsed surface muon beam with intensity of 1.2×10^6 μ^+/s and pulse repetition rate of 50 Hz. The basis of the technique has been described in detail previously [10,11]. Briefly, the surface muon beam is thermalized in a hot tungsten foil of optimized thickness. The muons that diffuse to the surface can be thermionically emitted to vacuum from the bulk metal as neutral muonium atoms, as the work function for muonium is much lower than that for the charged muon. The thermal muonium is then resonantly ionized through a two-photon 1S→2P→unbound process by a pulsed nanosecond laser to gain "free" muons with mean kinetic energy of only 0.2 eV.

2. Details of the experimental setup

Fig. 1 shows the layout of the experiment as it is set up at the RIKEN-RAL muon facility. The experimental setup for performing μSR measurements with LE-μ^+ consists of a laser system, an ultrahigh vacuum beamline (ion optics) for efficient transport of LE-μ^+ and a well shielded compact μSR spectrometer with all the necessary data acquisition electronics. Most of the laser parameters, as well as the parameters of the ion optics and tungsten target temperature can be remotely controlled and monitored from a dedicated control cabin.

2.1. Laser system

The binding energy of the electron in muonium is 13.6 eV. We believe that the most efficient laser ionization can be achieved through two-photon resonant ionization via the 2P state. This requires using two laser beams of different wavelengths. Firstly, for the strongly allowed electric-dipole transition from the 1S to 2P state, tuneable radiation around 122 nm (Lyman-α, 10.2 eV) is required. The second laser beam, for the ionization from the 2P state,

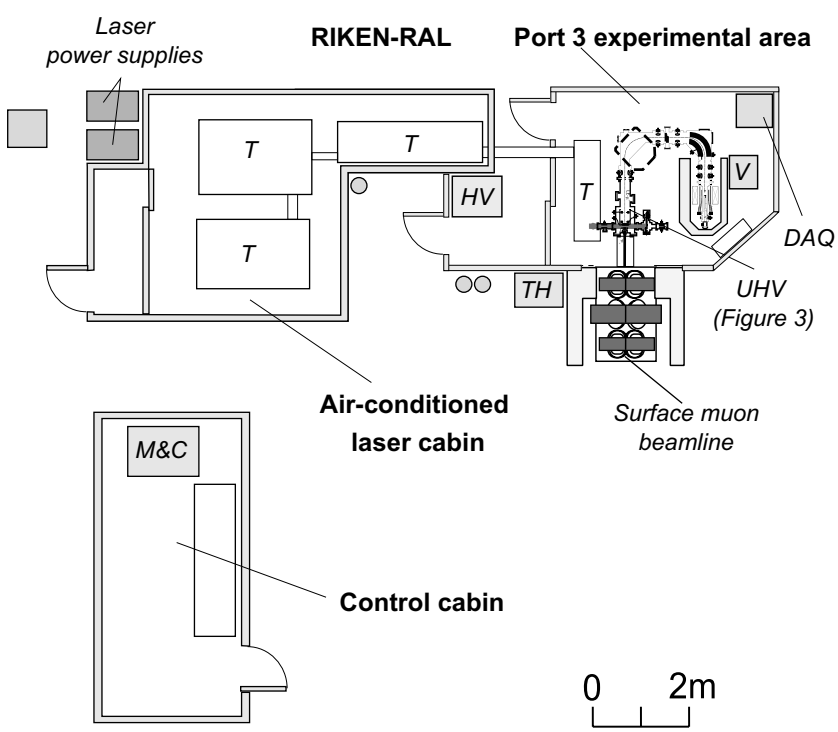

Fig. 1. Layout of the experiment to generate the low energy positive muons at ISIS RIKEN-RAL muon facility. T mark the optical tables with the laser system, UHV is the ultrahigh vacuum apparatus including the LE-μ^+ transport beamline (ion optics) and the μSR spectrometer, HV are the high voltage power supplies for the ion optics, DAQ is the data acquisition electronics for the μSR spectrometer and the computer control of the ion optics, V is the control rack for the ultrahigh vacuum system, TH is the high-current power supply for heating the tungsten foil, and M&C is the monitoring and remote control electronics of the important components of the laser system.

is required to have a wavelength shorter than 366 nm (3.4 eV) and, conveniently, the 355 nm laser beam generated as the third harmonic of a Nd:YAG laser can be used. The laser beam at 122 nm has not only to be tuneable, but also has to have a large bandwidth of about 200 GHz in order to cover the Doppler width of the thermal energy range of the muonium generated from the tungsten foil heated to 2000 K.

The 122 nm radiation is generated through a nonlinear frequency conversion process in a gaseous medium. Although this is inherently rather inefficient, being proportional to the third order nonlinear susceptibility $\chi^{(3)}$ tensor, there is no possibility to use birefringent nonlinear crystals, since none of the known nonlinear crystals is transparent at wavelengths below 190 nm. We are using a two-photon resonant sum-difference frequency mixing scheme in a phase-matched krypton gas [12]. This frequency conversion scheme unfortunately adds to the complexity of the laser system as it requires two laser beams, but it provides a large degree of tuneability and a high conversion efficiency ($\sim 10^{-4}$). The first laser is operating at 212.5 nm and is tuned to a two-photon resonance in Kr, while the second laser operating in the range of 810–850 nm provides the tuneability of the Lyman-α output and is designed to have sufficient bandwidth to cover the Doppler width of muonium. The wide tuneability of the output allows us to ionize under the same conditions not only muonium, but also hydrogen or deuterium. This provides a useful tool for testing the whole apparatus without need for the muon beam.

Fig. 2 shows a simplified schematic diagram of the laser system. The major part of laser system (generating the required beams at 355 nm, 212.5 nm and 810–850 nm respectively) is housed in an air-conditioned cabin connected via a duct with the rest of the apparatus at Port 3 of RIKEN-RAL muon facility (radiation area). The rest of the laser system is attached to the ultrahigh vacuum beamline and consists of beam steering and focusing optics, and a Kr–Ar cell for generating the Lyman-α radiation around 122 nm.

The details of the laser system and its layout have been described previously [13]. The main changes since this publication include a threefold increase of the output at 355 nm to 380 mJ/pulse by replacing the Spectra physics GCR-160 laser with a Continuum Powerlite 9025. At the same time we have also installed an image relay telescope in the path of the 355 nm beam to image the laser output to a distance of ~12 m at the Port 3 experimental area and thus ensure a more uniform intensity profile inside the ultrahigh vacuum beamline. Furthermore, an increase in the output pulse energy at 850 nm has been gained by adding a new 2-pass Ti:sapphire amplification stage at the output of the Continuum Mirage 800 laser and by introducing image relay telescopes in the path of the pump beams of the 4-pass Ti:sapphire amplifier. The resulting increase of the output pulse energy at 850 nm to 250 mJ/pulse and the significant improvement in the beam quality has lead to an increase in the available pulse energy at the

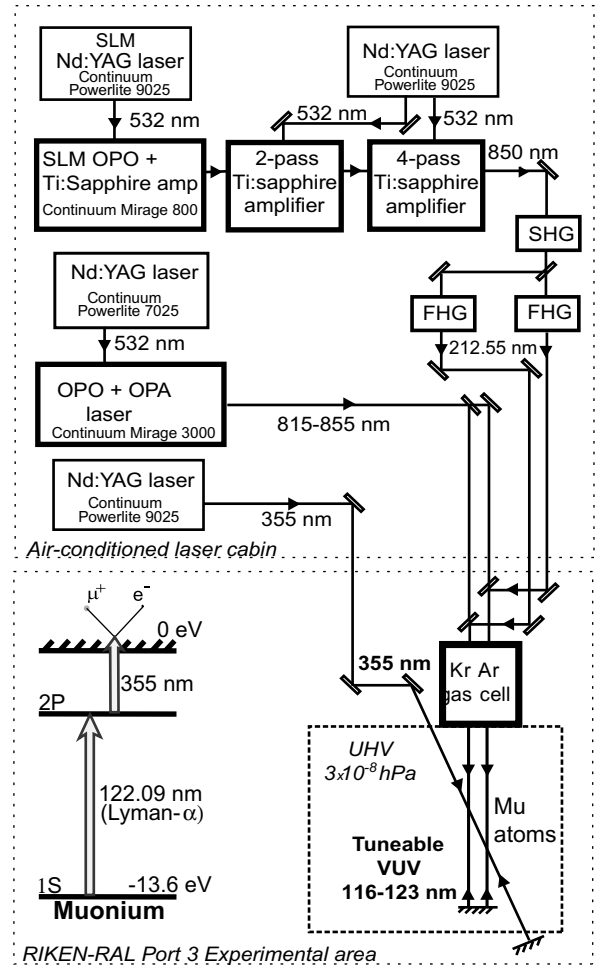

Fig. 2. Schematic diagram of the laser system used for resonant ionization of muonium. The image relay telescopes, beam focusing optics as well as the laser beam diagnostics are not shown in this diagram. SHG is 7 mm long BBO crystal (12 × 12 × 7 mm) for second harmonic conversion to 425 nm; FHG are temperature stabilised, 5 mm long, s-BBO crystals (12 × 12 × 5 mm) for conversion to 212.5 nm; SLM denotes single longitudinal mode operation. An inset shows a simplified energy level diagram of muonium to demonstrate the two-photon resonant ionization scheme used to gain μ^+ with mean energy of just 0.2 eV.

generated second harmonic at 425 nm by a factor of two (to 140 mJ/pulse). The 425 nm beam is then split into two beams and converted to 212.5 nm using two 5 mm long s-BBO crystals with conversion efficiency of approximately 15%. Although the s-BBO crystals are superior to BBO crystals at this wavelength, they still exhibit a significant nonlinear absorption at 212.5 nm, resulting in a temperature gradient between the input and exit faces of the crystal. This introduces a phase mismatch for the generated 212.5 nm beam that reduces the conversion efficiency. For this reason we have chosen to generate two separate 212.5 nm beams using two temperature stabilised s-BBO crystals and to cool the centre of the output face of the s-BBO by blowing nitrogen gas from a 1 mm diameter nozzle onto the crystal.

The current output parameters of the laser system are summarized in Table 1. The laser system has excellent long

Table 1
Summary of the laser output parameters

Wavelength	355 nm	212.5 nm	810–850 nm	116–123 nm (Lyman-α)
Pulse duration [FWHM]	10 ns	4 ns	12 ns	~4 ns
Pulse energy	380 mJ	10–12 mJ (×2 beams)	12 mJ (×2 beams)	>0.5 μJ (×2 beams)
Bandwidth	30 GHz	<2 GHz	180 GHz	180 GHz

term reliability. Stable 24 h/day operation can be sustained for up to 20 days, limited primarily by the lifetime of flashlamps used in the Nd:YAG lasers.

It is important to note that the laser system is operating at a repetition rate of only 25 Hz which means that only half of the muon pulses are used for LE-μ^+ generation. This limitation is due to strong thermal effects associated with operating high power solid state laser systems that make it difficult to build 50 Hz system with same pulse energy as achieved with the 25 Hz system.

2.2. LE-μ^+ transport beamline

Fig. 3 shows the layout of the LE-μ^+ beamline with the μSR spectrometer. The pulse of surface muons with momentum of 28 MeV/c enters the apparatus through a

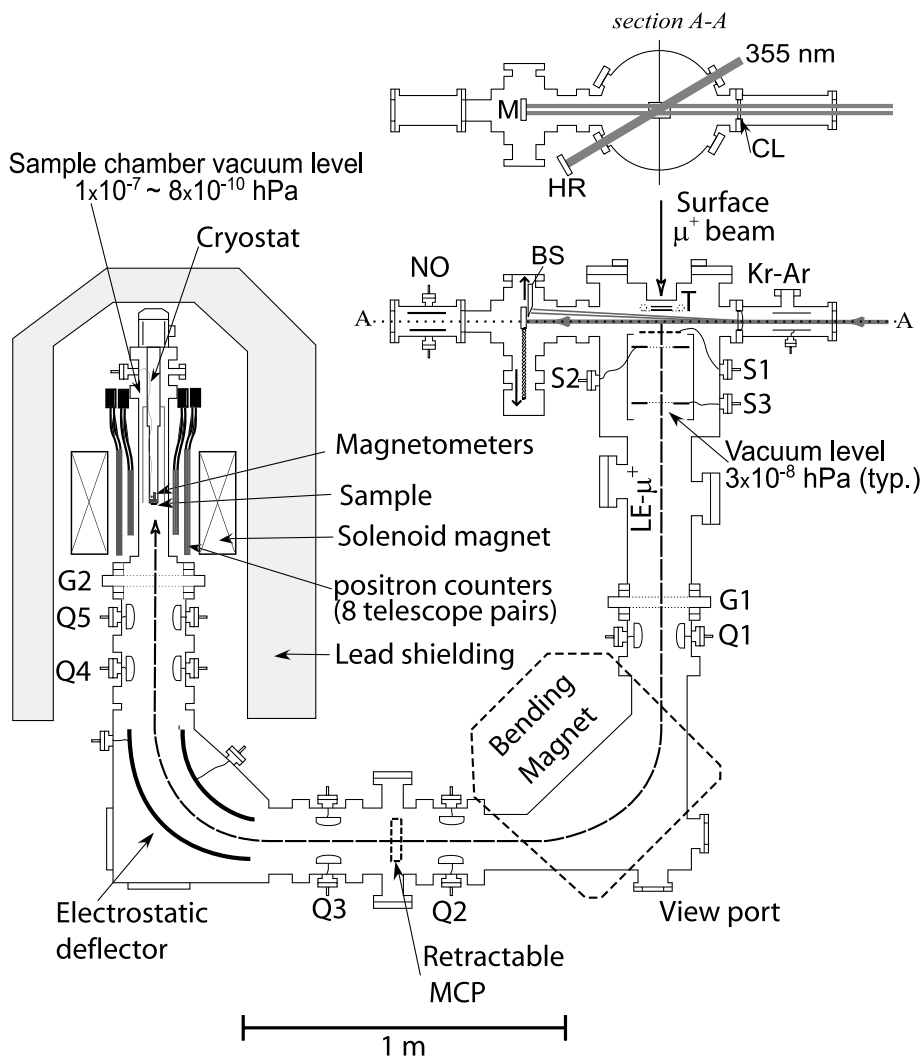

Fig. 3. Layout of the ultrahigh vacuum apparatus used to generate low energy positive muons (LE-μ^+) and to implant them in a sample. The sample is mounted on a cryostat inside a compact μSR spectrometer. Kr–Ar is the gas cell used to generate Lyman-α laser pulse by nonlinear frequency conversion, CL is the cylindrical lens window of the Kr–Ar gas cell, M is a remotely controlled, retractable retro-reflection mirror for the Lyman-α beams, HR is a remotely controlled dielectric retro-reflection mirror for 355 nm beam, BS is a remotely controlled knife-edge beam stop to protect M from 212.5 nm and 820 nm beams, NO is the ionization cell filled with NO gas for monitoring the Lyman-α pulse energy, T is the heated tungsten foil used to generate muonium, G1 and G2 are vacuum gate valves, S1–S3 are electrodes of SOA immersion lens, and Q1–Q5 are electrostatic quadrupole focusing elements. Section A-A shows the overlap of the laser beams in front of the tungsten foil.

50 μm thick stainless steel window and is first moderated by 20 μm thick tungsten foil and then by a 45 μm thick tungsten foil heated by DC current up to 2100 K. The function of the first foil is to shield the stainless steel window from the heat of the 45 μm tungsten target. The area of the tungsten target foil exposed to the muon beam is 40 mm (W) × 35 mm (H). The foils used were of 6 N purity (99.9999%W), manufactured by PLANSEE. The total thickness of the foils is optimized to stop a significant fraction of the incident beam near the rear surface of the hot foil which results in efficient emission of muonium atoms from the hot tungsten target.

Two sets of laser beams at 212.5 nm and 820 nm are each collinearly focused (with $f = 500$ mm plano-convex spherical lenses) into the cell filled with mixture of krypton and argon gas to generate two Lyman-α beams separated vertically by 10–15 mm. These then enter the ultrahigh vacuum chamber through a thin MgF_2 cylindrical lens (ROC = 78 mm; $f = 120$ mm @ 122 nm). The focusing optics shapes each of the Lyman-α beams to have (in front to the W foil) a width of only 1–2 mm (FWHM) in the horizontal plane and about 5–8 mm in the vertical plane. The two Lyman-α beams pass through a 14 mm wide gap between the tungsten target and the first extraction grid denoted as S1 and overlap the cloud of thermal muonium atoms about 5 mm from the target surface. The 355 nm beam is introduced to the beamline from the top at 30° from the Lyman-α beam and is shaped similarly to have a width of 3 mm by 25 mm. All laser beams are retro-reflected to maximize the ionization yield. Since the retro-reflecting mirrors are placed at the distance of 0.5 m, the width of the ionizing pulse is effectively broadened from 4 ns to 7 ns (FWHM). The overlap of the Lyman-α and 355 nm beams defines an interaction region with a volume of approximately 1 cm^3.

In order to protect the Lyman-α retro-reflecting mirror (Acton Research; Al reflector coated with MgF_2 protection layer; reflectivity @ 122 nm ~75%) from laser induced damage, the laser beams were aligned slightly off-centre on the cylindrical lens window. This dispersively separates the laser beams, so that the 212.5 nm and 820 nm beams can be blocked by a knife-edge beam stop placed in front of the Lyman-α reflector.

The LE-μ^+ generated by the laser ionization are initially extracted by a low gradient electrical field between the tungsten foil (held at 9.0 kV) and mesh electrode S1 (held at 8.8 kV). S1 is the first of three elements forming an SOA immersion lens [14] which then re-accelerates the LE-μ^+ to 9.0 keV. Such arrangement is necessary in order to minimize the energy variation of the re-accelerated LE-μ^+ beam. The SOA lens also focuses the collected LE-μ^+ to a tight spot of only 2.5 mm (FWHM) which is then imaged to the sample surface with the ion transport optics consisting of five electrostatic quadrupoles (Q1–Q5), a bending magnet and an electrostatic deflector. In this geometry the electrostatic deflector effectively rotates the muon spin polarization, which is originally anti-parallel to the momentum, by 90°. The muons implanted into the studied sample are therefore horizontally polarized with the spin perpendicular to the muon momentum.

The section of the beamline between the bending magnet and the electrostatic deflector houses a retractable position-sensitive microchannel plate detector (ROENTDEK DLD-80). This is used either for checking the yield and profile of the LE-μ^+ beam or for measuring D^+ yield when optimizing the performance of the apparatus by ionizing the residual deuterium dissociated by the hot tungsten target.

The total transmission efficiency of the beamline has not been measured, but it is worth noting that there is a significant loss of muons due to decay. The overall path length from the tungsten target to the focus at the sample chamber is 3.9 m and the time-of-flight for 9.0 keV muons is 1.15 μs, resulting in ~40% loss of LE-μ^+ due to decay. We are planning to increase the acceleration voltage to 18 keV. This will extend the range of available implantation energies and reduce the loss through decay in flight to about 28%.

2.3. Sample chamber and μSR spectrometer

The sample chamber, which has a diameter of 100 mm and a length of 540 mm, can be isolated from the rest of the ultrahigh vacuum beamline to allow changing of samples. The vacuum level in the apparatus is typically 3×10^{-8} hPa when measured in the vicinity of the heated tungsten foil. The vacuum level in the sample chamber can be as low as 8×10^{-10} hPa several days after a sample change. Experiments with LE-μ^+can be started approximately 6 h after the sample change when the vacuum level reaches about 1×10^{-7} hPa. Samples for the μSR studies can be mounted on a closed circuit two-stage helium cryostat (Iwatani HE-05 with cooling power of 0.5 W at 4 K) capable of cooling samples to about 10 K. Alternatively, the sample chamber can accommodate a position-sensitive microchannel plate detector (ROENTDEK DLD-40) that is used to check the focusing of the LE-μ^+ beam. The energy of the muons implanted into the sample can be continuously varied from zero to 18 keV by applying voltage in the range of +9.0 kV to −9.0 kV directly onto the sample holder, which is isolated from the cryostat finger by 10 mm thick disc of sapphire.

Around this small sample chamber we have built a compact μSR spectrometer designed with the aim of providing a very high signal-to-noise ratio. The sample chamber is surrounded by a close arrangement of eight telescope pairs of plastic scintillation counters covering a solid angle of 80% of 4π sr. These detectors are inserted inside a solenoid type coil with a magnetic length of 260 mm providing magnetic field with strength of up to 60 mT parallel to the muon momentum and perpendicular to the spin. The magnetic field homogeneity at the field value of 8 mT over a distance of 40 mm along the magnet's axis is below 500 ppm. The field homogeneity measured at 3 mT in the transverse direction over a 10 mm radius is below

100 ppm. In-built into the magnet are also coils for compensating external magnetic fields of up to 250 μT (2.5 G) in any direction. The spectrometer can be therefore used for transverse field TF-μSR measurements as well as measurements in zero external magnetic field (ZF-μSR). During the ZF-μSR measurements the zero field compensation can be monitored using three single axis fluxgate magnetometers (Bartington Instruments MAG01-H F-probes). These are mounted on the sample holder immediately behind the sample. The zero field condition can thus be maintained at a level 0.1 μT (1 mG) over a period of several days.

To make meaningful μSR measurements with the relatively low LE-μ^+ rates currently achieved requires a very low background. The combination of the bending magnet and electrostatic deflector provides selection of the transported ions by mass and energy, respectively. This, together with lead shielding with thickness of 100–200 mm around the scintillation detectors and the sample chamber, provides excellent background suppression to less than 0.012 counts over the 15 μs period after each muon pulse. In our case, when the laser is operating at half the repetition rate of the ISIS accelerator, the signal-to-noise ratio can be further increased by subtracting the fixed background of the laser-off spectrum from the laser-on spectrum. This allows us to observe LE-μ^+ decay to at least 6 muon lifetimes after the implantation, see Fig. 4.

3. Experimental results

3.1. Dependence of LE-μ^+ yield on laser pulse energy

The high efficiency of thermal muonium production from the surface muon beam makes this method potentially capable of cooling surface muons to eV energies with efficiency as high as 10^{-2}. However, it is currently limited by the available laser pulse energy, especially at the Lyman-α frequency. The relative measurement of the energy of the Lyman-α pulse is made by passing the Lyman-α beam through an NO gas cell at a pressure of

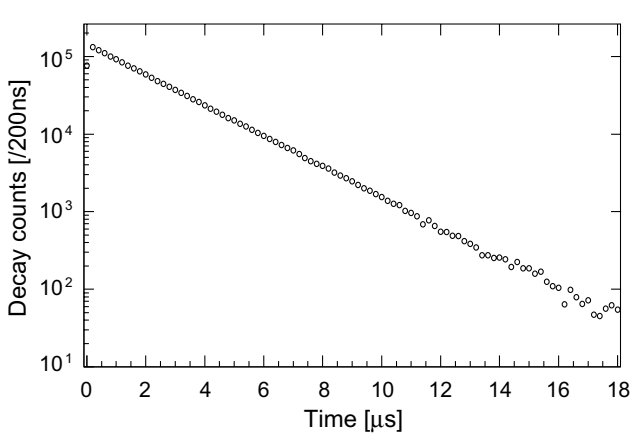

Fig. 4. Histogram of positron counts originating from LE-μ^+ decay in the sample chamber.

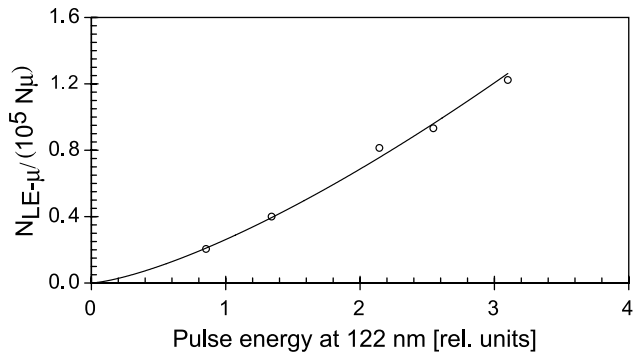

Fig. 5. Dependence of the overall efficiency of LE-μ^+ generation on the pulse energy of the Lyman-α at 122 nm. The efficiency is determined as a ratio of the number of LE-μ^+ delivered at the sample position per laser pulse $N_{LE-\mu}$ and the number of incident surface muons per pulse N_μ. Relative values of pulse energy at 122 nm are determined from photoionization signal in NO gas. A single 122 nm beam was generated by focusing 212.5 nm beam with energy of 12 mJ and 820 nm beam with pulse energy of 13 mJ into the Kr–Ar cell. In this measurement the 122 nm beam was not retro-reflected and was instead absorbed in the NO gas cell. The energy of the 355 nm pulse measured at the output of the laser was 280 mJ.

6.5 hPa and measuring the photoionization current [15]. Fig. 5 shows the observed dependence of the LE-μ^+ yield on the Lyman-α energy. It shows that even though the laser beam overlaps just a small fraction of the muonium cloud (~1 cm^3), the Lyman-α intensity is still not sufficient to saturate the Doppler broadened 1S–2P transition. We do not currently have a detector in our setup to measure the absolute pulse energy of the generated Lyman-α and can only make a rough estimate of ~1 μJ/pulse (total of 2 beams) based on the integrated ionization current of the NO gas cell. Given the beam size in front of the tungsten foil we can estimate the peak intensity to be in the region of several kW/cm^2, still below the expected saturation intensity (for 200 GHz Doppler broadening) of 5 kW/cm^2.

Significant improvement (beyond an order of magnitude) of the Lyman-α pulse energy with the existing laser system is not currently envisaged. Our previous investigations have shown that process of Lyman-α generation in krypton gas is saturated [13] and gains achieved by compensating for the phase mismatch in krypton gas with argon gas are not as high as originally anticipated. Our measurements show that for the phase-matched Kr–Ar mixture the conversion efficiency from the UV beam at 212.5 nm is fixed at approximately the 10^{-4} level. For pulse energy E of the 212.5 nm beam in the range of 2–14 mJ the Lyman-α energy is increasing approximately as $E^{0.8}$. Therefore, further increase of Lyman-α energy and consequently a higher LE-μ^+ yield should be possible by increasing the pulse energy of the 212.5 nm beam. Further improvement of the LE-μ^+ yield can be also expected from an increase of the pulse energy of the 355 nm beam judging from the energy dependence of the LE-μ^+ yield shown in Fig. 6.

With the current laser parameters, the overall conversion efficiency including transport losses is 3×10^{-5} and about 15 μ^+/s are observed at the sample chamber – a significant improvement on our first result in 2001 of

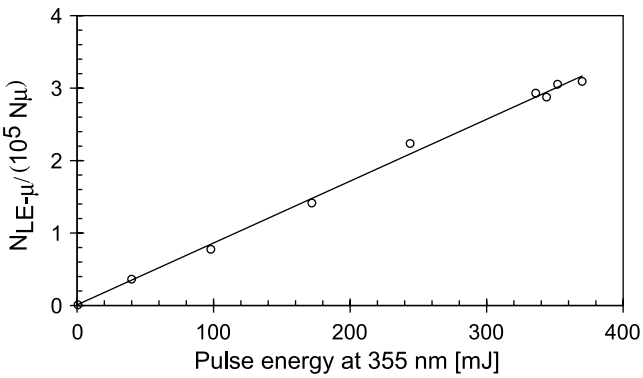

Fig. 6. Dependence of the overall efficiency of LE-μ^+ generation on the laser pulse energy at the wavelength of 355 nm. The laser pulse energy was measured at the output of the laser; the actual pulse energy at 355 nm delivered inside the ultrahigh vacuum system is about 35% lower due to absorption in air and losses on mirrors and optical windows. Estimated intensity of 355 nm beam inside the vacuum system is about 30 MW/cm^2 (at maximum laser output of 380 mJ) Compared to the measurement shown in Fig. 5, the muonium excitation to the 2P state was increased by using two 122 nm beams vertically separated by 15 mm that were retro-reflected by VUV mirror with reflectivity $R = 0.75$. Each of the 122 nm beams was generated from 9.0 mJ at 212.5 nm and 9.5 mJ at 820 nm.

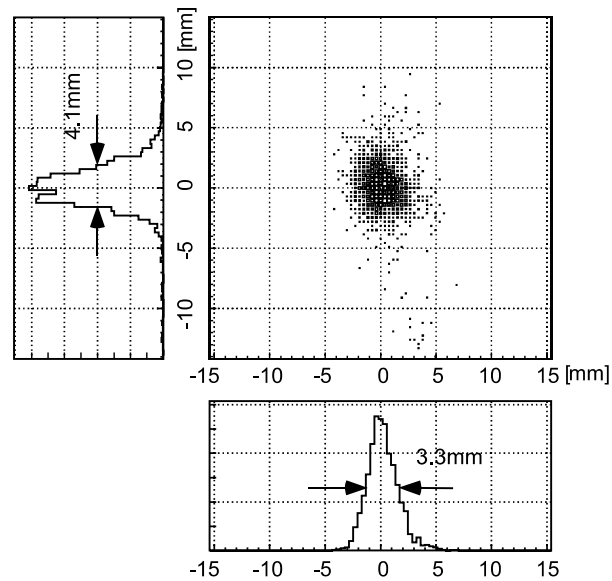

Fig. 7. Plot of the 9 keV LE-μ^+ beam spot at the sample position measured with a position-sensitive microchannel plate detector with a resolution of 0.5 mm.

0.03 μ^+/s [13]. This has allowed us to perform simple μSR experiments and demonstrate the feasibility of this method for pulsed muon sources.

Of as much importance as the LE-μ^+ rate is the capability to focus the muons into a small spot at the sample, since for the μSR investigations with the LE-μ^+ only small samples may be available. While the full-width at half-maximum (FWHM) diameter of the incident surface muon beam is 35 mm, the FWHM diameter of LE-μ^+ beam is about 10 times smaller. The beam spot was measured with a position-sensitive MCP (ROENTDEK DLD-40) placed at the sample position. The spot-size measured at the focus of the LE-μ^+ beam accelerated to 9.0 keV is shown in Fig. 7. Gaussian fitting in the horizontal and vertical directions yields FWHM of 3.3 mm and 4.1 mm, respectively.

3.2. Pulse duration

A particularly important advantage of using the short laser pulse to ionize muonium is the improvement of the muon pulse structure and the capability of having an external control over the triggering of the LE-μ^+. The surface muon beam at RIKEN-RAL has a double-pulse structure consisting of ~80 ns (FWHM) pulses separated by 320 ns. The short laser pulses ionizing muonium atoms are triggered with an optimum delay of about 400 ns relative to the surface muon pulse. This delay allows the muonium – having the mean thermal velocity of 20 mm/μs – to evaporate to a few millimetres away from the tungsten target and reach its maximum density in the laser beam volume. The arrival time of the muons at the sample is determined by the timing of the laser pulse plus a fixed delay corresponding to a time-of-flight (TOF) through the apparatus. As the muonium cloud is expanding relatively slowly, the laser timing and consequently the LE-muon timing can be varied around the optimum value by several hundred nanoseconds at the expense of the LE-μ^+ rate (the rate is approximately halved by delaying the muonium ionization by 400 ns relative to the optimum delay). As the laser itself can be externally triggered with 1 ns accuracy, this feature opens a possibility to perform new μSR measurements requiring precise triggering of the muon implantation and synchronization with pulsed sample excitation. The time of muon implantation relative to an external laser trigger is known to within the pulse width of the LE-μ^+ in the TOF spectrum, which is below 10 ns. This pulse width of the LE-μ^+ is completely independent of the complicated pulse structure of the surface muon beam and is determined primarily by the duration of the laser pulse and partly also by the acceleration voltage. The time-of-flight (TOF) spectrum measured at sample position for 9.0 keV muons is shown in Fig. 8.

3.3. Energy resolution

The generation of LE-μ^+ based on the laser ionization of thermal muonium makes it possible to generate beams with extremely narrow energy resolution, as the LE-μ^+ have kinetic energy of only 0.2 eV after ionization. This is significantly lower than the intrinsic energy resolution of the LE-μ^+ generated by moderation in van der Waals bound solids, where the epithermal muons escape the moderator with rms energy spread of about 15 eV. If the high energy resolution of the order of several eV can be maintained through re-acceleration, transport and deceleration up to the sample, ultra-thin films or surfaces could be studied using the μSR technique with ~1 nm resolution. The depth

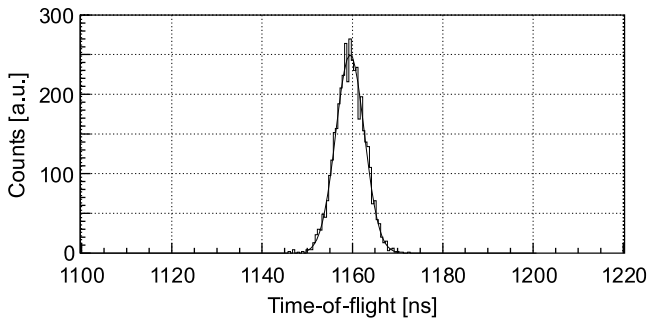

Fig. 8. Time-of-flight histogram of the 9.0 keV LE-μ^+ detected by microchannel plate detector at the sample position. Time zero corresponds to muonium ionization by the laser pulses. Gaussian fit to this histogram yields FWHM pulse duration of 7.5 ns.

resolution in the sample depends mainly on the density of the material and the muons' struggling in it. To give an example, for muons implanted in Al with a mean energy of 20 eV and a standard deviation of 10 eV, the calculation using the Monte Carlo code TRIM.SP [16,17] gives the mean penetration depth to be just 0.7 nm with a spread of 0.7 nm. Reducing the energy resolution below 10 eV, however, does not significantly reduce the width of the muon implantation profile as it is determined by muons' struggling in Al. In this respect the depth resolution of the order of 1 nm should be achievable by either method of LE-μ^+ generation but only using a pulsed muon beam. For continuous muons beams, such as available at PSI, it is necessary to determine the muon implantation time in order to construct the μSR spectrum. This requires inserting a thin foil into the LE-μ^+ beam and thus broadening the energy resolution at the sample to ~400 eV [10].

In our experimental setup achieving the energy resolution of several eV at the sample is possible. The energy variation of the re-accelerated LE-μ^+ depends on the differences in the potential seen by the individual muons at the point of laser ionization relative to the S1 electrode. The difference in electrostatic potential over the 14 mm gap between the tungsten foil and S1 is therefore kept low (at only 200 V). The differences in electrostatic potential seen by the individual muons are mainly arising due to:

(a) the width of the ionization region determined by the overlap of the Lyman-α and 355 nm beams (including the retro-reflected beams), which is of the order of 2 mm (FWHM), thus contributing to the standard deviation of the muon energy with ~13 eV;
(b) the uneven distance between tungsten foil and S1 arising from bending of the heated tungsten foil into the gap – this reduces the gap of 14 mm at the edges of the foil to ~12 mm at its centre – contributing to the standard deviation of the muon energy with ~4 eV;
(c) any differences in aligning the two Lyman-α beams at the same distance from S1 and parallel to S1 – also contributing to the energy variation with ~4 eV.

The effect of the pulse-to-pulse pointing stability of the laser beams is below 1 eV level. These contributions give an estimate of the energy resolution of the extracted LE-μ^+ as $\sigma_E = 14$ eV (33 eV at FWHM). The energy resolution can be improved by reducing the extraction field between the tungsten foil and S1 and possibly also by reducing the width of the interaction region, though this would make alignment of the retro-reflected Lyman-α beams more difficult.

3.4. Test μSR experiments

To demonstrate the feasibility of using the pulsed beam of LE-μ^+ for μSR measurements we have measured some simple muon spin precession spectra in transverse magnetic field. Despite the relatively low rate of 15 μ^+/s implanted into the sample, up to 10^6 positrons originating from the muon decay in sample ($\mu^+ \rightarrow e^+ + \nu_e + \bar{\nu}_\mu$) can be detected per day by the scintillation counters of our μSR spectrometer. The number of detected positrons as a function of time after the muon implantation in each of the detector pairs was recorded in eight histograms $N_i(t)$ ($i = 1, \ldots, 8$). Let us assume for simplicity of the explanation that the muons are implanted into a metal, where muonium can not be formed, and subjected to a static magnetic field oriented perpendicular to the initial muon spin direction. The time dependence recorded in these histograms then corresponds to the exponential muon decay with the muon lifetime τ_μ modulated by the free muon spin precession with Larmor precession frequency ω_μ, and by the spin relaxation function $G(t)$ and can be expressed in the form

$$N_i(t) = N_{0i} e^{-t/\tau_\mu}[1 + A_\mu G_\mu(t)\cos(\omega_\mu t + \varphi_i)] + N_i^{BG}(t) \quad (i = 1, \ldots, 8), \tag{1}$$

where N_{0i} is normalization constant for each of the detector pairs. The initial phases φ_i are fixed by the geometry to the initial phase φ_1 ($\varphi_i = \varphi_{i-1} + \pi/4$ for $i = 2, \ldots, 8$). The background contribution and $N_i^{BG}(t)$ to the signal can in our setup be determined from every second muon pulse when laser is off and the low energy muons are not incident on the sample. The spin relaxation function depends on the distribution of the local magnetic fields seen by the implanted muons. For example, if local fields have a Lorentzian distribution then $G_\mu^L(t) = e^{-\lambda t}$. Simultaneous fitting of all eight histograms then allows determining the parameters ω_μ, λ and the initial amplitude of the precession signal A_μ, the so-called diamagnetic asymmetry. It follows from the angular distribution of the positrons originating from the muon decay that the maximum value of A_μ when integrated over all positron energies is equal to 1/3 if the implanted muons are initially 100% spin polarized. The asymmetry values in the vicinity of 0.2–0.25 are typical for μSR instruments, depending on the setup.

The LE-μ^+ generated by the ionization of muonium, however, are only 50% spin polarized and the asymmetry is therefore expected to be half of the value typical for other μSR instruments. This polarization loss is a result

of the interaction with the electron spin in the muonium atom. The muonium bound state is formed with equal probabilities for the muon and electron spins to be either parallel (ortho-muonium) or anti-parallel (para-muonium). In the case of anti-parallel spins, the hyperfine interaction causes rapid depolarization of the initial muon spin [18,19] and hence only half of the low energy muons obtained by the muonium ionization are spin polarized.

In our first experiment we have implanted LE-μ^+ with energy of 9 keV into a 20 mm diameter silver sample at room temperature. The initial diamagnetic asymmetry A_μ determined by fitting the data from the eight detector pairs was $A_\mu^{Ag} = 10.11 \pm 0.23\%$ with no observable spin depolarization ($G(t) = 1$).

In order to visualize the muon spin precession signal we have divided the detectors into two opposing groups of four detectors and added the positron signals in each group into one histogram and subtracted the background signal determined from the "laser off" data. The μSR asymmetry spectrum from these two histograms $N_{G1}(t)$ and $N_{G2}(t)$ is plotted in Fig. 9 simply as

$$a_0(t) = \frac{N_{G1}(t) - N_{G2}(t)}{N_{G1}(t) + N_{G2}(t)}. \quad (2)$$

The amplitude of the oscillations determined from these two histograms is consistent with multiplying the initial diamagnetic asymmetry A_μ by a geometrical factor of 0.653, reflecting the fact that positron signal is integrated over an angle of π rather than π/4 radians.

In our next test experiment we have used the pulsed LE-μ^+ beam for depth-resolved μSR measurement analogous to the measurements of Morenzoni et al. [17] of a thin metallic film sample coated on an insulator. The purpose of the experiment was to demonstrate the control over the implantation energy and the mean implantation depth. The principle of the experiment is described in detail by Morenzoni et al. [17] and relies on the fact that the stopping site of muons can be determined from the amplitude of the spin precession signal of the "free" diamagnetic muon (diamagnetic asymmetry) in the sample. The muons that penetrate through the metallic layer and thermalize in the insulator substrate will mostly form muonium. For the half of the muons that form para-muonium the polarization will be rapidly lost due to the hyperfine interaction and for the rest that forms ortho-muonium the transitions between muonium triplet states in a weak transverse magnetic field B will yield a single Larmor precession frequency of $\omega_{Mu} = 87.619\ \text{Mrad/mT} * B$, about 100 times faster than the muon precession of $\omega_\mu = 0.852\ \text{Mrad/mT} * B$. By choosing the field B sufficiently large, so that $2\pi/\omega_{Mu}$ is much shorter than the binning interval of the positron decay histogram, the muonium spin precession signal can be averaged out. The muons that formed muonium will then show in the measured signal as a loss of the diamagnetic asymmetry, which will be reduced proportionally to reflect the remaining number of diamagnetic muons in the sample.

Our sample, placed at the focus of the LE-μ^+ beam (~4 mm FWHM), was an optically flat SiO_2 substrate, 20 mm in diameter, coated by sputtering with a pure Al layer with a nominal thickness of 40 nm. The experiment was performed at the room temperature under UHV conditions at a pressure of $\approx 10^{-9}$ hPa in a 4 mT (40 G) external magnetic field transverse to the muon spin.

The implantation profile for muons – taking into account the muon energy, the incidence angle and the sample density – can be accurately calculated using the Monte Carlo code TRIM.SP. Fig. 10 shows the calculated implantation profiles in the sample for several implantation energies.

Fig. 11 shows the measured initial amplitude of the diamagnetic muon precession (diamagnetic asymmetry) as a function of the muon implantation energy. This measured dependence is in a good agreement with the calculated fraction of diamagnetic muons using the TRIM.SP program. The measured asymmetry is a sum of contributions from diamagnetic muons that have thermalized in the Al layer and from the small fraction of muons in the SiO_2 substrate that did not form muonium; there is also a small background contribution from muons that thermalized in any metal parts outside the sample, e.g. in the metal ring holding the edges of the sample. For muons that penetrate the

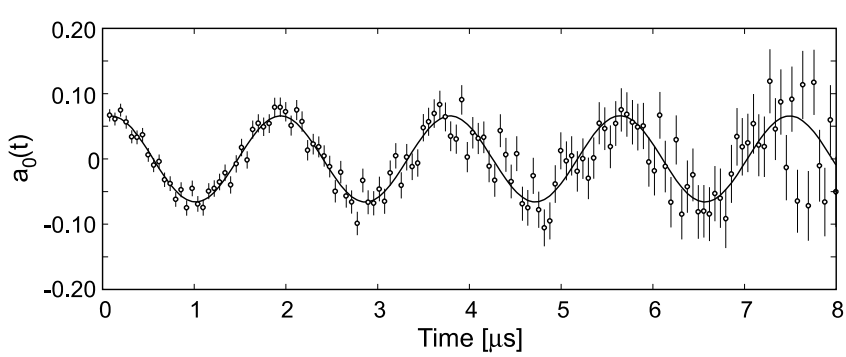

Fig. 9. Muon spin precession signal measured in pure Ag sample with 9 keV LE-μ^+. The signal represents asymmetry in the positron decay spectrum observed between two opposing groups of four detectors. Since the signals from four detectors in each group were added into one histogram the amplitude of the oscillations reflecting the spin precession of μ^+ is effectively reduced. The diamagnetic asymmetry A_μ as defined in Eq. (1) for eight individual detectors can be obtained by dividing the amplitude of the spin precession signal shown here by a factor of 0.653.

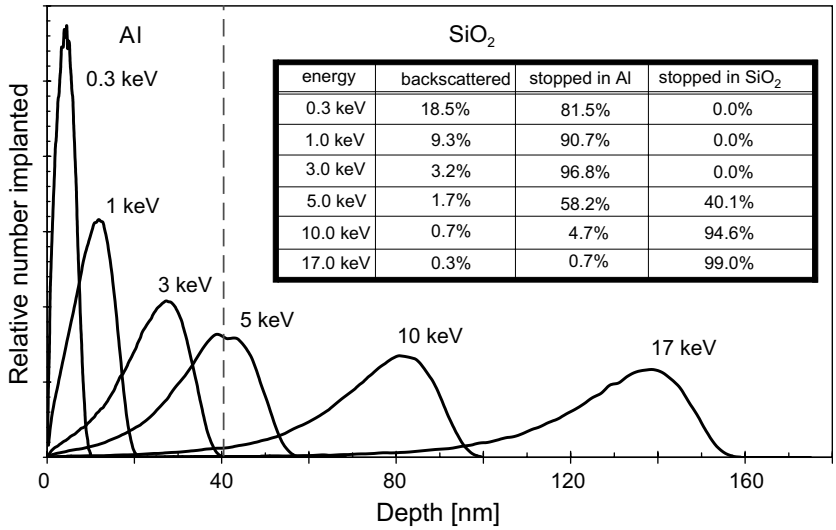

energy	backscattered	stopped in Al	stopped in SiO_2
0.3 keV	18.5%	81.5%	0.0%
1.0 keV	9.3%	90.7%	0.0%
3.0 keV	3.2%	96.8%	0.0%
5.0 keV	1.7%	58.2%	40.1%
10.0 keV	0.7%	4.7%	94.6%
17.0 keV	0.3%	0.7%	99.0%

Fig. 10. The implantation profiles for LE-μ^+ in 40 nm thick Al layer on SiO_2 substrate calculated for different implantation energies using TRIM.SP code. Calculation assumes narrow Gaussian energy distribution of the incident muons with a standard deviation of $\sigma_E = 14$ eV and the incidence angle being perpendicular to the sample surface with $\sigma_\alpha = 5$.

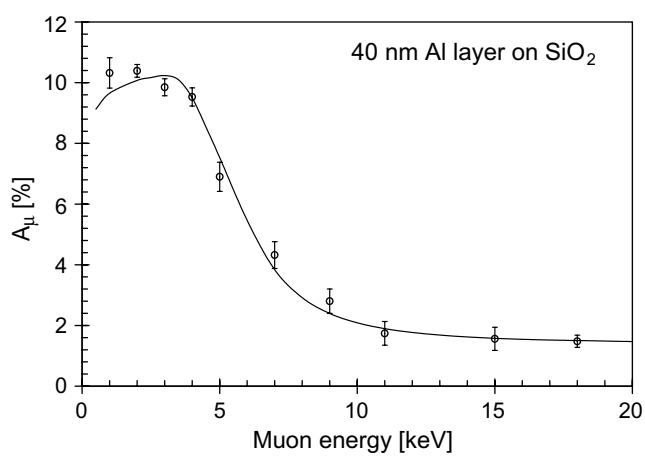

Fig. 11. Energy dependence of the asymmetry of the diamagnetic muon A_μ measured in SiO_2 sample coated with 40 nm thick Al layer. For muon implantation energies below 4 keV the muons are mostly stopped in Al layer and remain as free muons and consequently the measured asymmetry approaches the maximum observable asymmetry A_{max} of the μSR spectrometer. With increasing implantation energy, the muons penetrate into SiO_2 substrate (see Fig. 10) where most of the stopped muons form muonium. This results in proportional loss of the measured diamagnetic asymmetry A_μ. The solid line is the expected energy dependence of A_μ derived from the muon stopping profiles calculated using the TRIM.SP code.

SiO_2 with residual energy below 5 keV there remains a relatively large fraction that does not form muonium and the diamagnetic asymmetry contribution from the SiO_2 substrate is therefore energy dependent. We have used this energy dependence $A_{SiO_2}(E)$ measured in [[17] (Fig. 8)] to determine the contribution from free diamagnetic muons in the SiO_2 substrate to the measured asymmetry. The mean residual energies of muons after passing through the 40 nm Al layer as well as the numbers of muons implanted to SiO_2 and Al layer were calculated using the TRIM.SP code for 10^5 incident LE-μ^+. In the calculation we have assumed standard deviation of the incident muon energy to be $\sigma_E = 14$ eV and the standard deviation of the incidence angle from the normal incidence to be $\sigma_\alpha = 5°$. We have included in the calculation small thickness variation of the Al layer with a standard deviation of 2 nm. We have not considered any Al_2O_3 oxide layer that might have formed on the surface of the sample as we have seen no reduction of the measured asymmetry for low implantation energies. The TRIM.SP calculation predicts reflection of a fraction of muons at low incident energies (about 9% of the total at 1 keV and as much as 30% at 0.1 keV). Upon reflection there is a high probability that the muon captures an electron and forms muonium and this should result in a corresponding reduction of the measured diamagnetic asymmetry. We have not, however, seen this reduction for muons implanted at energy of 1 keV, given the low statistics we have accumulated for this data point.

The background contribution to the asymmetry from the muons stopping in metal parts outside the sample was determined from the diamagnetic asymmetry of $1.5 \pm 0.2\%$ measured at 18 keV. At this energy all of the incident muons are implanted in SiO_2, where about 0.09 ± 0.01 of them will remain as diamagnetic muons [17] contributing to the asymmetry with $1.0 \pm 0.1\%$. The background contribution to the measured asymmetry is then estimated to be $0.5 \pm 0.2\%$, corresponding to about 0.045 of the incident muons stopping outside of the 20 mm diameter of the sample.

It should be noted that at room temperature the muons implanted in the Al layer will rapidly diffuse throughout the metal layer, but not necessarily into the SiO_2 substrate. For the muon energies in the range of 1–4 keV, when most of the muons are implanted into the Al layer, we have observed a small spin relaxation rate $\lambda = 0.10\ \mu s^{-1}$

independent of the implantation energy (within our experimental error). It was found by measurements in bulk Al that pure Al gives rise to no depolarization in the temperature range of 0.1–300 K [20]. Our own measurements with 18 keV muons implanted into a 500 nm thick pure Al sample at room temperature also show minimal relaxation rate $\lambda = 0.03 \pm 0.02\ \mu s^{-1}$. The small relaxation observed in our 40 nm thick Al layer is therefore most likely related to a small fraction of muons diffusing across the Al/SiO_2 interface. The structural disorder and imperfections at the layer interface in samples prepared by sputtering significantly hinder the diffusion across the interface, as was observed for the Cr/Au interface prepared by sputtering [21].

The short pulse duration of the LE-μ^+ generated by the laser ionization of muonium allows us to measure very high precession frequencies and extend the dynamic range for pulsed μSR to measure processes on a timescale ranging from nearly 10 ns to more than 10 μs. For a Gaussian pulse shape with FWHM width of τ_p the amplitude A of the harmonic component at frequency f will reduce by a factor

$$\frac{A(f)}{A(0)} = \exp\left(-\frac{\pi^2\tau_p^2 f^2}{4\ln 2}\right). \tag{3}$$

We have measured this frequency response using the orthomuonium spin precession signal in a transverse field of up to 3 mT (30 G). LE-μ^+ with energy of 15 keV were implanted into the Al (40 nm) coated SiO_2 sample. If the positron decay time histograms are binned in intervals shorter than $2\pi/\omega_{Mu}$ the fitting function (Eq. (1)) has to include an additional term describing the muonium spin precession

$$\begin{aligned} N_i(t) = {} & N_{0i}e^{-t/\tau_\mu}[1 + A_\mu G_\mu(t)\cos(\omega_\mu t + \varphi_i) \\ & + \frac{A_{Mu}}{2} G_{Mu}(t)\cos(\varpi_{Mu} t + \varphi_i^{Mu})] \\ & + N_i^{BG}(t) \quad (i = 1, \ldots, 8), \end{aligned} \tag{4}$$

where the amplitude of the muonium precession signal is written in the usual convention as one half of the initial muonium asymmetry A_{Mu}, since the other half of the muonium asymmetry is not observed due to fast depolarization. On implantation, the sum of A_μ and A_{Mu} must equal the maximal experimentally observable asymmetry A_{max} which we have determined from our measurement of diamagnetic asymmetry in pure metal sample ($A_{max} = A_\mu^{Ag} = 10.11 \pm 0.23\%$). As we have determined in the measurements shown in Fig. 11, the diamagnetic asymmetry from the free diamagnetic muons at 15 keV is $1.56 \pm 0.38\%$, the expected muonium asymmetry A_{Mu} is then $8.55 \pm 0.44\%$. The ratio of the observed muonium asymmetry and the expected muonium asymmetry is then plotted against the muonium precession frequency in Fig. 12. As expected from the short duration of the LE-μ^+ pulse, fast spin precession frequencies and fast relaxation rates can be observed; although this is admittedly limited by the relatively low count rate. With about 10^6 muon decay events detected, the muonium spin precession at 28 MHz could be clearly observed with muonium asymmetry reduced by 25% compared to the asymmetry measured at low frequency. By fitting the measured data points with frequency dependence according to Eq. (3) the pulse width τ_p can be determined as $\tau_p = 12.7 \pm 2.0$ ns. This value is somewhat higher than the LE-μ^+ pulse duration determined from the time-of-flight spectrum (Fig. 8) as it also includes various optical and electronics delays involved in detecting the positrons from the muon decay in the μSR spectrometer.

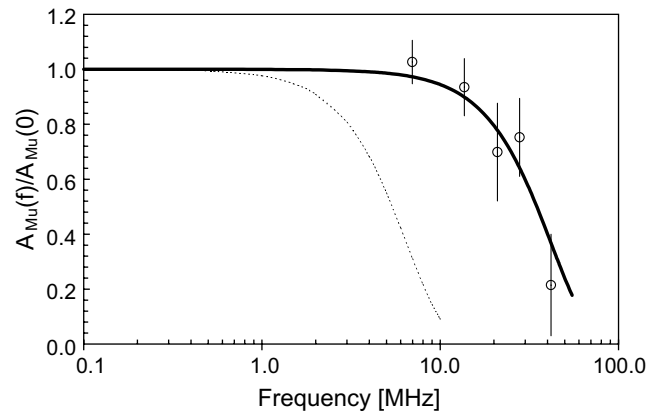

Fig. 12. Frequency response plot of the LE-μ^+ μSR apparatus as measured using muonium spin precession signal in SiO_2 sample. The data points show the ratio of the measured muonium asymmetry to the expected muonium asymmetry obtained for several precession frequencies from 7 MHz up to 42 MHz. The solid line represents fit to the data points with frequency dependence according to Eq. (3) yielding $\tau_p = 12.7 \pm 2.0$ ns. For comparison, the dotted line shows the frequency response for $\tau_p = 82$ ns, equivalent to FWHM duration of the ISIS surface muon pulse.

4. Conclusions

An experimental setup has been constructed at RIKEN-RAL muon facility to perform depth-resolved μSR measurements on nanometre scale with pulsed ultra low energy muons. Several μSR experiments have been carried out to demonstrate the characteristics of the apparatus. The parameters of the pulsed low energy muon beam are summarised in Table 2. The efficiency of the surface muon beam cooling to eV level is comparable to the method using the cryogenic moderator (of $\sim 3 \times 10^{-5}$). The efficiency of thermal muonium production is, however, of the order of 10^{-2}. As Figs. 5 and 6 demonstrate, the laser pulse energy is not yet sufficient to ionize all muonium atoms, even though the laser beams overlap only a small fraction of the generated thermal muonium cloud. Therefore, there is a clear prospect that with development of a new and more intense VUV laser source, the efficiency of LE-μ^+ production could be increased by up to two orders of magnitude. The muonium ionization method of LE-μ^+ generation has distinct advantages for pulsed operation. The LE-μ^+ implantation in the sample can be externally triggered with nanosecond accuracy that makes it possible to perform μSR experiments where the muon implantation is synchronised with a sample

Table 2
Present characteristics of the pulsed LE-μ^+ beam and of the μSR spectrometer

Low energy muon beam parameters	
Intensity at sample	15 μ^+/s
Beam spot diameter at sample	4 mm (FWHM)
Energy at W target region	0.2 eV
Energy after reacceleration	0.1–18 keV
Energy uncertainty after reacceleration	$\sigma_E \approx 14$ eV
Pulse repetition rate	25 Hz
Pulse duration in TOF spectrum at 9.0 keV	7.5 ns (FWHM)
μ^+ spin polarization	≈50%
μSR spectrometer parameters	
Solid angle covered by detectors	80% of 4π sr
Maximum instrumental asymmetry of μSR spectrometer	10.1%
Maximum measurable spin precession frequency	≈40 MHz
Sample cryostat temperature range	10–300 K
Transverse magnetic field range	0–60 mT
Zero field compensation	≈0.1 μT

excitation. The LE-μ^+ pulse duration is reduced to only 7.5 ns (measured at FWHM), which is in fact as short as the time resolution for the LE-μ^+ implantation at continuous muon source [22]. This short pulse duration is independent of the initial pulse structure of the incident surface muon beam, which would be of particular advantage if this method of LE-μ^+ generation was used at the new J-PARC Muon Science Facility where each muon pulse will consist of two bunches each of 100 ns duration and separated by as much as 600 ns [23].

Acknowledgements

The authors would like to thank F. Pratt for his advice on analysing the data from μSR measurements and his keen interest in our experiments. We are also very grateful to E. Morenzoni and W. Eckstein for kindly providing us with the TRIM.SP code. We are also indebted to R. Scheuermann for his contribution to the construction of the ion beamline. The construction of this low energy muon facility was possible due to large financial support of KEK-MSL and UT-MSL (for purchasing the high power lasers and ion optics), and of RIKEN (for construction and operational costs). This research was partially supported by the Grant-in-Aid for Scientific Research (A)16206005, (B)11559019, (C)11650052 and Grant-in-aid for Exploratory Research 16656295 by the Ministry of Education, Culture, Sports, Science and Technology of Japan.

References

[1] S.J. Blundell, Spin-polarized muons in condensed matter physics, Contemp. Phys. 40 (1999) 175.
[2] Special issue on μSR: muon spin rotation, relaxation or resonance, in: R.H. Heffner, K. Nagamine, (Eds.), J. Phys.: Condens. Matter, 16 (2004).
[3] K. Nagamine, Y. Miyake, K. Shimomura, P. Birrer, J.P. Marangos, M. Iwasaki, P. Strasser, T. Kuga, Ultraslow positive-muon generation by laser ionization of thermal muonium from hot tungsten at primary proton beam, Phys. Rev. Lett. 74 (1995) 4811.
[4] D.R. Harshman, A.P. Mills Jr., J.L. Beveridge, K.R. Kendall, G.D. Morris, M. Senba, J.B. Warren, A.S. Rupaal, J.H. Turner, Generation of slow positive muons from solid rare-gas moderators, Phys. Rev. B 36 (1987) 8850.
[5] E. Morenzoni, F. Kottmann, D. Maden, B. Matthias, M. Meyberg, Th. Prokscha, Th. Wutzke, U. Zimmermann, Generation of very slow polarized positive muons, Phys. Rev. Lett. 72 (1994) 2793.
[6] K. Träger et al., Production of pulsed ultra slow muons and first μSR experiments on thin metallic and magnetic films, Physica B 289–290 (2000) 662.
[7] E. Morenzoni, T. Prokscha, A. Suter, Applied muon science: novel perspectives in nano-science, Nucl. Phys. B (Proc. Suppl.) 149 (2005) 73.
[8] T. Prokscha, E. Morenzoni, C. David, A. Hofer, H. Glückler, L. Scandella, Moderator gratings for the generation of epithermal positive muons, Appl. Surf. Sci. 172 (2001) 235.
[9] T. Matsuzaki, K. Ishida, K. Nagamine, I. Watanabe, G.H. Eaton, W.G. Williams, The RIKEN-RAL pulsed muon facility, Nucl. Instr. and Meth. A 465 (2001) 365.
[10] P. Bakule, E. Morenzoni, Generation and applications of slow polarized muons, Contemp. Phys. 45 (2004) 203.
[11] Y. Miyake, K. Shimomura, S. Makimura, Y. Matsuda, P. Bakule, K. Nagamine, Ultra-sensitive detection of hydrogen isotopes by Lyman-α RIS, J. Nucl. Sci. Technol. 39 (2002) 287.
[12] J.P. Marangos, N. Shen, H. Ma, M.H.R. Hutchinson, J.P. Connerade, Broadly tuneable vacuum-ultraviolet radiation source employing resonant enhanced sum-difference frequency mixing in krypton, J. Opt. Soc. Am. B 7 (1990) 1254.
[13] P. Bakule, Y. Matsuda, Y. Miyake, P. Strasser, K. Shimomura, S. Makimura, K. Nagamine, Slow muon experiment by laser resonant ionization method at RIKEN-RAL muon facility, Spectrochim. Acta B 58 (2003) 1019.
[14] K.F. Canter, P.H. Lippel, W.S. Crane, A.P. Mills Jr., in: A.P. MillsJr., W.S. Crane, K.F. Canter (Eds.), Positron Studies of Solids, Surfaces, and Atoms, World Scientific, Singapore, 1984, p. 199.
[15] J.A.R. Samson, D.L. Ederer, Vacuum ultraviolet spectroscopy, Experimental Methods in the Physical Sciences, Academic Press, London, 2000.
[16] W. Eckstein, Computer Simulation of Ion–Solid Interaction, Springer, Berlin, 1991.
[17] E. Morenzoni, H. Glückler, T. Prokscha, R. Khasanov, H. Luetkens, M. Birke, E.M. Forgan, Ch. Niedermayer, M. Pleines, Implantation studies of keV positive muons in thin metalic layers, Nucl. Instr. and Meth. B 192 (2002) 254.
[18] V.W. Hughes, D.W. McColm, K. Ziock, R. Prepost, Muonium. I. Muonium formation and larmor precession, Phys. Rev. A 1 (1970) 595.
[19] M. Senba, Spin dynamics of positive muons during cyclic charge exchange and muon slowing down time, J. Phys. B 23 (1990) 1545.
[20] K.W. Kehr, D. Richter, J.-M. Welter, O. Hartmann, E. Karlsson, L.O. Norlin, T.O. Niinikoski, A. Yaouanc, Muon diffusion and trapping in aluminum and dilute aluminum alloys: Experiments and comparison with small-polaron theory, Phys. Rev. B 26 (1982) 567.
[21] H. Luetkens, J. Korecki, E. Morenzoni, T. Prokscha, N. Garif'yanov, H. Glückler, R. Khasanov, F.J. Litterst, T. Slezak, A. Suter, Diffusion of muons in metallic multilayers, Physica B 326 (2003) 545.
[22] T.K. Paraïso, E. Morenzoni, T. Prokscha, A. Suter, Geant4 simulation of low energy μSR experiments at PSI, Physica B 374–375 (2006) 498.
[23] Y. Miyake et al., J-PARC Muon Science facility with use of 3 GeV proton beam, Nucl. Phys. B (Proc. Suppl.) 149 (2005) 393.